Algorithm Theoretical Basis Document for the Joint Single Footprint Retrieval Algorithm (JoSFRA)

Fredrick W. Irion, John M. Blaisdell[†], Eric J. Fetzer, Evan Fishbein, Alexander Goodman, Brian H. Kahn, Evan Manning, Ruth Monarrez, Mathias M. Schreier, Heidar Th. Thrastarson, Qing Yue

Jet Propulsion Laboratory, California Institute of Technology
Pasadena, CA

[†]Science Applications International Corporation
NASA Goddard Space Flight Center, Greenbelt, MD

March 2024

Document Version 2.0

Algorithm Version: 2.0

Prepared for the National Aeronautics and Space Administration

©2024 California Institute of Technology. Government sponsorship acknowledged.

Revision History

Document Version	***Algorithm Version***	***Revision Date***	***Changes / Comments***
1.0	2.0	2023-12-18	Initial Release – Peer review pending
2.0	2.0 (JOSFRA_twoStep.L1B.V6tuning.0.08.16)	2024-03-06	Additions and clarifications per external review

Table of Contents

List of Symbols

ε_{cld}	cloud emissivity
ε_{surf}	surface emissivity
$\mathbf{F}$	forward-model radiance
P_{cldtop}	cloud-top pressure
P_{layer}	model layer pressure
P_{surf}	surface pressure
r_{eff}	effective cloud particle radius
$\mathbf{S}_a$	a priori covariance
$\mathbf{S}_\varepsilon$	radiance noise covariance
T_{atm}	temperature profile
T_{cldtop}	cloud-top temperature
T_{surf}	surface temperature
τ_{cld}	cloud optical depth (at 0.55 μm)
$\hat{\mathbf{x}}$	"full" state vector (containing more elements than $\hat{\mathbf{z}}$ below, and used in forward model)
ξ	surface emissivity logistic parameter (see Eq. 16)
$\mathbf{y}$	vector of measured radiances
$\mathbf{z}$	"true" state vector
$\hat{\mathbf{z}}$	"retrieval" state vector
$\mathbf{z}_a$	a priori retrieval state vector

Abstract

This Algorithm Theoretical Basis Document (ATBD) describes the Joint Single Footprint Retrieval Algorithm (JoSFRA) applied to Atmospheric Infrared Sounder (AIRS) thermal infrared spectra. In this version, JoSFRA retrieves atmospheric parameters, including temperature and water vapor profiles, surface temperature, cloud-top temperature, cloud optical depth, and effective cloud particle size. By putting clouds in the forward model and avoiding combining footprints in "cloud-clearing," retrievals are made at the scale of the AIRS native footprint (~13.5 km at nadir) without the loss of horizontal resolution from combining spectra of adjacent footprints. An optimal-estimation scheme forms the basis of the retrieval, with cloud a priori from coincident retrievals by the co-located Moderate Resolution Imaging Spectroradiometer (MODIS).

1. Introduction

The Atmospheric Infrared Sounder (AIRS) instrument is a thermal infrared grating spectrometer, providing global measurements of atmospheric temperature and water vapor profiles (among other parameters) for use within weather forecast models, assimilation models, process studies, and climate studies. (See, for example, Aumann et al., 2003, and Chahine et al., 2006.) AIRS was launched May 4, 2002 in sun-synchronous, polar orbit on the EOS Aqua satellite and began routine measurements on August 31, 2002 at an altitude of 705 km. It has been in near-continuous operation to date.

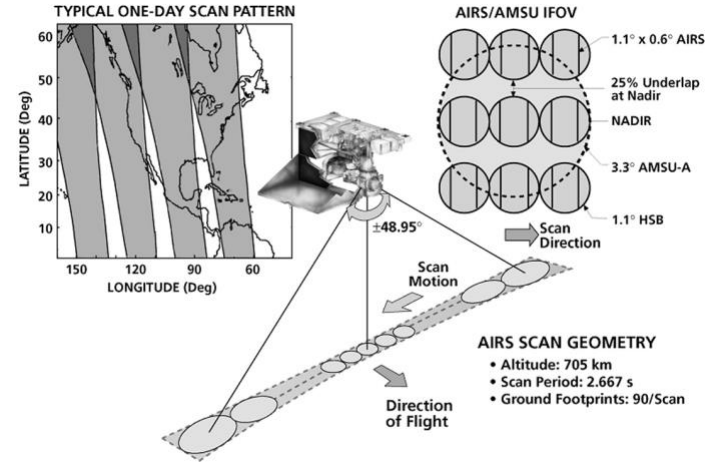

Figure 1: Geometry of AIRS/AMSU/HSB observation from the AIRS instrument. (From Aumann et al., 2003).

AIRS delivers approximately 2.9 million spectral observations every 24 hours, with 2378 channels between 3.7 and 15.4 μm (although in practice, only a subset of these channels are used for retrievals). AIRS was designed for co-located measurements with the microwave Humidity Sounder of Brazil (HSB; failed in February, 2003), and the Advanced Microwave Sounding Unit (AMSU) microwave instrument. Nine AIRS observations (each with nadir horizontal resolution of ~13.5 km) are in a 3 x 3 grid over a single AMSU observation with a nadir horizontal resolution of ~45 km (Figure 1). The design of the AIRS/AMSU/HSB system was to overcome the complication of cloud contamination in infrared retrievals. This complication is illustrated in Figure 2, which samples the effect of clouds on adjacent spectra observed by AIRS. The basic premise of the AIRS operational retrieval was that all fields (temperature, water vapor, surface temperature etc.) were homogeneous over the AMSU field-of-regard except for the cloud parameters, which would be variable among the nine AIRS footprints. Regression calculations would be applied to a 3x3 ensemble of AIRS spectra to estimate a "cloud-cleared" spectrum, upon which retrievals would be made assuming no clouds.

This would be the case if AMSU data were used in conjunction with AIRS spectra or if AIRS spectra were used alone.

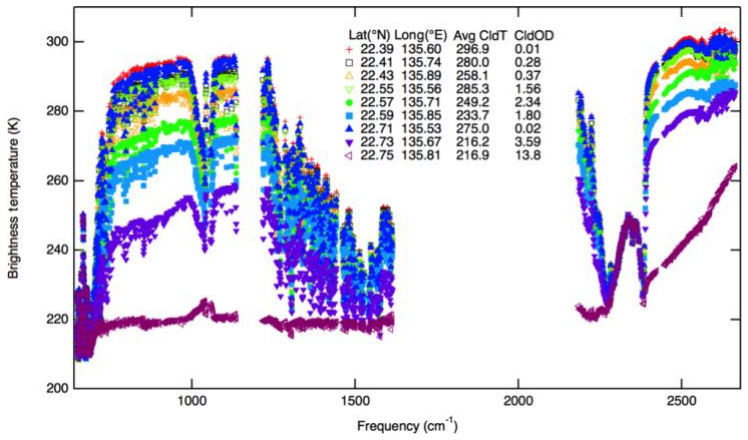

Figure 2: AIRS level 1b brightness temperature observations of adjacent cloudy spectra. Data are from daytime Granule 44, 6 September 2002. Average cloud-top temperatures and cloud optical depths are estimated from coincident MODIS L2 retrievals, averaged on the AIRS spatial response function. (From Irion et al., 2018)

While this approach greatly simplifies forward modelling, an obvious drawback is that the horizontal resolution of the retrievals is reduced from the AIRS measurements; an AIRS footprint at 13.5 km at nadir is used for a ~45 km footprint retrieval of temperature, moisture etc., with only effective cloud fraction and cloud top temperature on the native AIRS resolution. When combining AIRS data, and assuming constant non-cloud quantities, horizontal gradients can be masked particularly for water vapor with its shorter horizontal length scales compared to temperature (e.g., Kahn and Teixeira, 2009). Since the design stage era of AIRS in the 1990's, increased computing power coupled with advances in modelling cloudy spectra have allowed greatly improved hyperspectral infrared retrievals of atmospheric parameters on a cloudy scene. To be sure, this means a more complicated forward modelling process and does not solve the issue of thermal infrared retrieval of parameters below a thick cloud. However, it does allow retrievals to be made on the footprint of an infrared observation, without losing horizontal resolution from regressing spectra to a zero-cloud state.

Herein, we describe the Joint-Operational Single Footprint Retrieval Algorithm (JoSFRA). This effort retrieves atmospheric parameters from nadir thermal infrared spectra in their native horizontal footprint, using clouds in the forward model, and without recourse to a cloud-cleared state. The overall algorithm uses an optimal-estimation scheme (Rodgers et al., 2000) for retrieval. Forward modelling is done by using a delta-4-stream (D4S) approach for cloud transmissivities (Ou et al., 2013) incorporated into the operational AIRS forward model, the Standalone AIRS Radiative Transfer Algorithm (SARTA; Strow et al., 2003). For a priori parameters, National Center for Environmental Prediction (NCEP) forecasts are used for

atmospheric and skin temperatures (T_{atm}, T_{surf}), water vapor, and surface pressure. A priori cloud-top temperature (T_{cldtop}), optical depth (τ_{cld}) and daytime effective particle radius (r_{eff}) are derived from co-located Moderate Resolution Infrared Sounder (MODIS) retrievals (Platnick et al., 2017) averaged over the AIRS spatial footprint. The a priori optical depth is derived from the MODIS cloud emissivity (which is produced for both daytime and nighttime), and not from the MODIS cloud optical depth, which is a daytime-only product.

1.1 Changes to algorithm from Irion et al. (2018)

This ATBD has similarities to Irion et al. (2018), which described an earlier version of this retrieval. It is not necessary for the reader of this ATBD to be familiar with Irion et al., but for the convenience of those who are familiar with that paper, we describe significant changes to the algorithm below.

1. Instead of all parameters being retrieved simultaneously, the retrieval is now performed in two steps. In "Step One," simultaneous retrieval of the temperature and CO_2 profiles, surface temperature, cloud properties and emissivity (over land) is performed, mostly on the 14 μm CO_2 band and window regions, with ozone and water vapor profiles also retrieved as "interferent" gases. (The 9.6 μm band of ozone is not used in the retrieval.) In "Step Two," the water vapor profile a priori reverts back to the NCEP forecast, the channel selection is modified, and only the water vapor profile is retrieved, using the retrievals from Step One as fixed parameters.
2. The a priori temperature and water vapor profiles were changed from European Center for Medium-Range Weather Forecasting (ECMWF) forecasts to those provided by the National Center for Environmental Prediction (NCEP). Profiles are still spatially and temporally interpolated to the AIRS observation. In converting NCEP relative humidity to specific humidity or water mixing ratio, the equations of Murray (1967) are used for calculation of the saturation pressures. In a holdover from the earlier version of the retrieval, the equations of Wagner and Pruß (2002) are used for calculation of the output relative humidity.
3. Co-location and averaging of MODIS cloud data on the AIRS spatial footprint is now done using an adaptation of the fast method of Wang et al. (2016).

4. A priori cloud optical depth is now calculated from the MODIS cloud emissivity, which is available day and night, instead of using the daytime-reported MODIS cloud optical depth and assuming a fixed optical depth a priori at night.
5. In determining whether a scene is clear or not, or has cirrus, liquid or mixed-phase cloud but an unknown cloud-top temperature, we also use ice cloud and liquid cloud "scores" as calculated by the method reported by Jin and Nasiri (2014) and Kahn et al. (2014) in addition to the use of MODIS cloud mask flags.
6. The optical depth of a forward model layer containing a cloud top was previously calculated assuming that the cloud occupied the entire layer. The layer optical depth is now calculated with the layer separated into a clear sublayer overlaying a cloudy sublayer (with the boundary being the cloud top pressure).
7. Surface emissivities were previously entered as fixed parameters. They are now retrieved over land at selected hinge frequencies, but remain as fixed parameters over water. Land emissivity is retrieved if the land fraction of the scene is greater than 1% as reported by the AIRS Level 1b spectral data set. The a priori land emissivities are calculated by simple linear interpolation to the center of the AIRS footprint, and are no longer averages weighted by the AIRS spatial response function.
8. Since the retrieval is now two step, quality-control criteria have been modified to have two separate outputs – one output for the "Step One" retrievals (temperature, clouds, CO_2, O_3, and emissivity if over land), and a separate output for the "Step Two" retrieval (H_2O). If a Step One retrieval fails, then no Step Two retrieval is attempted. It is also possible for a Step One retrieval to pass quality control while a Step Two retrieval does not.

1.2 Notes on the retrieval of carbon dioxide and ozone

The retrieval of the temperature profile in the thermal infrared generally relies on the thermal sensitivity of CO_2 spectral lines, but there can also be retrieval sensitivity to changes in the actual CO_2 abundance. While retrieval sensitivity to CO_2 is small compared to T_{atm}, early testing indicated a small improvement in temperature retrievals compared to radiosondes when the CO_2 amount was retrieved simultaneously with temperature. CO_2 retrievals are thus included in JoSFRA output, but we again note that the sensitivity is small, and the accuracy and precision of

these retrievals have not been well evaluated. We therefore do not recommend use of JoSFRA CO_2 retrievals for further research purposes.

For ozone, we avoid channels in the 9.6 μm O_3 band as its inclusion often results in a failure for the retrieval to converge. (As noted by Kulawik et al., 2006, for the Tropospheric Emission Sounder retrieval, difficulty in finding a global minimum can happen when retrieving all species at once.) However, including ozone in the retrieval (through its weak absorption within the 14 μm CO_2 band) but not including the strong 9.6 μm band improves the overall fitting, with fewer failed retrievals. We therefore retrieve O_3 only as an "interferent" gas solely to improve the fitting within the 14 μm CO_2 region, and these O_3 retrievals are not recommended for further study. Retrieval of ozone can be revisited in future versions of JoSFRA.

2. Single-footprint retrieval algorithm

The JoSFRA retrieval process proceeds in two steps, with simplified block diagrams in Figures 3 and 4. For convenience, blocks are annotated with the section numbers of this ATBD where more information can be found.

2.1 Optimal estimation cost function

The mathematical basis for optimal estimation retrievals is described by Rodgers (2000). For JoSFRA, implementation is similar to that of the Tropospheric Emission Spectrometer (TES; Bowman et al, 2006), but with significant differences in the treatment of clouds. The retrieval

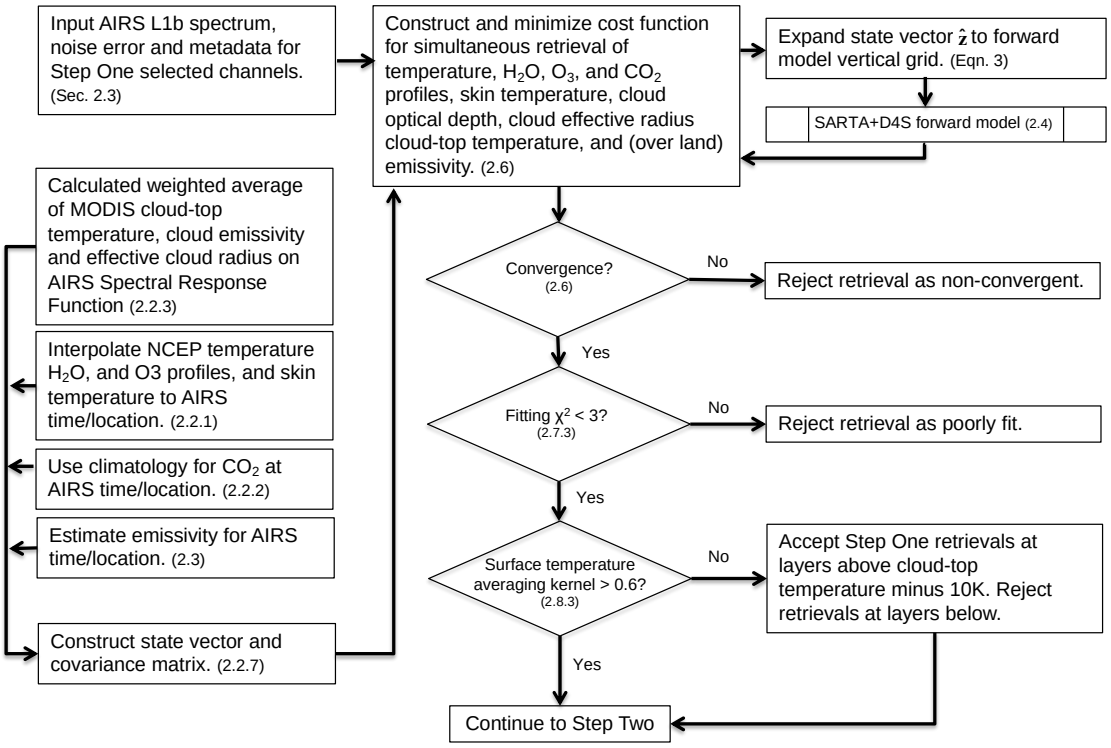

Figure 3: Simplified flowchart for Step One of JoSFRA retrieval. Notations refer to sections within this ATBD.

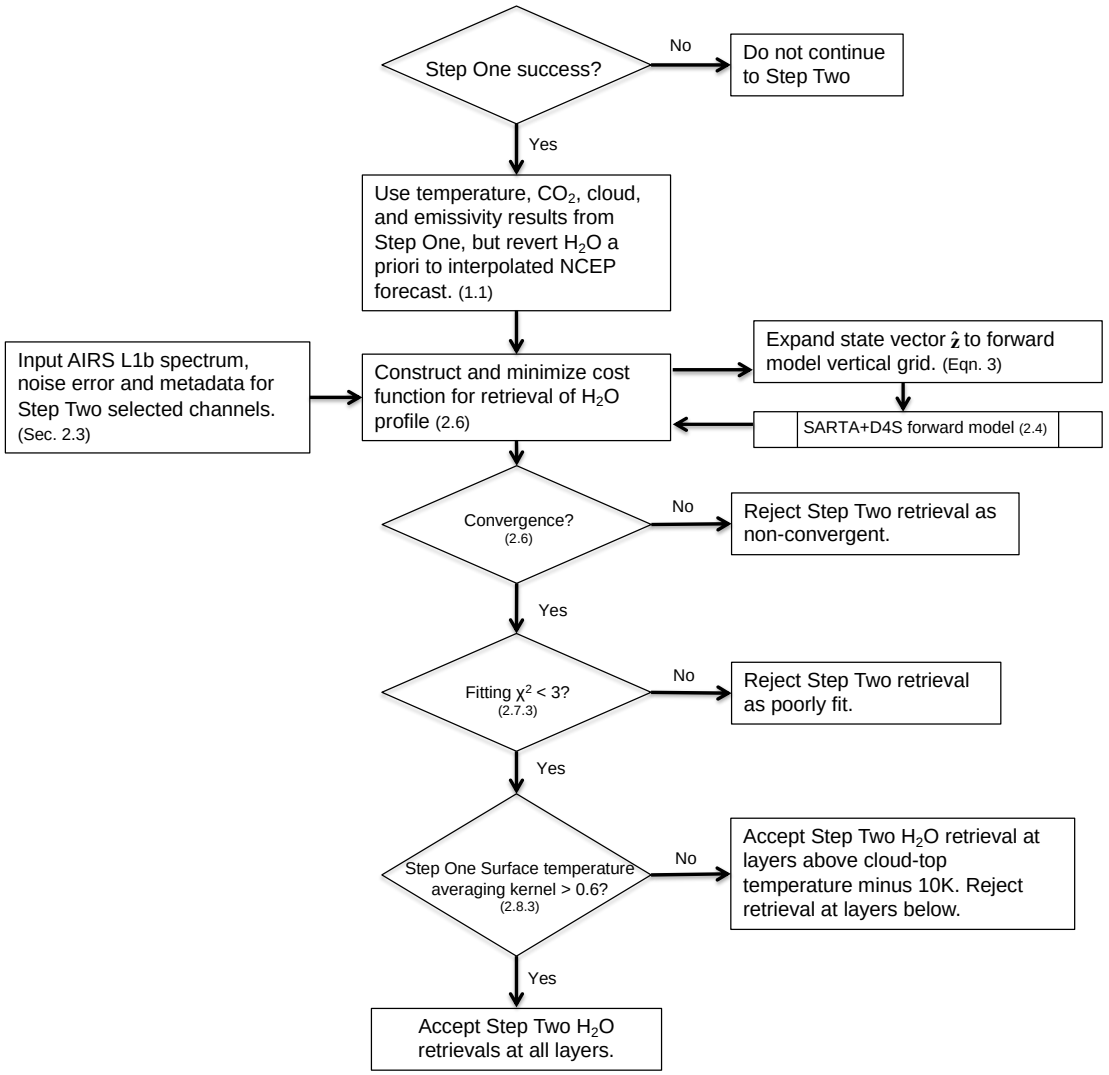

Figure 4: Simplified flowchart for Step Two of JoSFRA retrieval. Notations refer to sections within this ATBD.

algorithm minimizes the difference between an observed and a forward-modelled radiance, subject to a quadratic constraint, through the cost function:

$$C = (\mathbf{y} - \mathbf{F}(\hat{\mathbf{x}}, \mathbf{b}))\mathbf{S}_{\mathcal{E}}^{-1}(\mathbf{y} - \mathbf{F}(\hat{\mathbf{x}}, \mathbf{b}))^{-1} + (\hat{\mathbf{z}} - \mathbf{z}_{\mathrm{a}})\mathbf{S}_{a}^{-1}(\hat{\mathbf{z}} - \mathbf{z}_{\mathrm{a}})^{-1} \quad (1)$$

where:

y is the vector of measured radiances,
F($\hat{\mathbf{x}}$, **b**) is the forward-model radiance,
$\hat{\mathbf{x}}$ is the "full" state vector, described below,
b contains additional variables needed (but not retrieved) and observational metadata (e.g., scan angle) for calculating radiances,

$\hat{\mathbf{z}}$ is the "retrieval" state vector, described below,
$\mathbf{z}_a$ is the a priori retrieval state vector,
$\mathbf{S}_\varepsilon^{-1}$ is the inverse radiance noise covariance, and
$\mathbf{S}_a^{-1}$ is the inverse covariance of the a priori $\mathbf{z}_a$.

(Note that we accent a retrieved quantity with a caret, e.g., $\hat{\mathbf{z}}$, to distinguish it from the "true" quantity, **z**.)

The measurement error covariance, $\mathbf{S}_\varepsilon$, contains the radiance noise error covariance from the instrument. It can also contain other *random* radiance error sources, such as those from forward model calculations, although these have not been included in this version. The a priori state vector, $\mathbf{z}_a$, is also the first guess in a retrieval. The full state vector, $\hat{\mathbf{x}}$, has as many elements for each retrieved profile constituent (T_{atm}, H_2O, O_3 and CO_2) as there are layers in the forward model at or above ground, plus those for retrieved scalar quantities, surface temperature (T_{surf}), cloud-top temperature (T_{cldtop}), cloud optical depth[1] (τ_{cld}) and effective cloud particle radius (r_{eff}), and, over land, surface emissivity (ε_{surf}) at selected hinge frequencies. There are a maximum of 100 layers filled in the forward model from the surface upwards, on its fixed pressure grid with level pressures from 1100 to 0.1 hPa (as described in Strow et al., 2003). The pressure layers are constructed as the log-mean of the upper and lower pressure levels:

$$P_{layer} = \frac{P_2 - P_1}{ln(P_2/P_1)} \qquad (2)$$

Following Bowman et al. (2006), the forward-model layer gridding must be fine enough for calculation of the observed radiance, but is usually much finer than the vertical resolution of a retrieved profile. The retrieval state vector, **z**, has a reduced number of layers, which varies by constituent, to reflect a lower vertical resolution. (A maximum 42 layers are retrieved for T_{atm}, 28 for H_2O, 10 for CO_2 and 9 for O_3.) These layers are listed in Table 1, however we note that the retrieval state vector, **z,** always includes the lowest *complete* forward model layer (that is, the lowest layer that does not contain the surface.) For "partial" layers where the surface pressure

[1]The optical depth reported, $\tau(c)$, is that at 0.55 μm. The optical depth, $\tau(\nu)$ at some wavenumber ν can be determined by the relationship $\tau(\nu) = \tau(c) <Q_{ext}(\nu)>/2$, where $<Q_{ext}(\nu)>$ is the mean extinction efficiency for the spectral channel. Extinction efficiencies are from Baum et al. (2007) and their use in thermal infrared retrievals of cirrus parameters is in Ou et al. (2013).

falls between forward model pressure levels, the temperature and mixing ratio profiles are not retrieved, but are instead extrapolated by log pressure from the complete model layers above to the partial layer below.

The retrieved state vector, $\hat{\mathbf{z}}$, is mapped to the full state vector, $\hat{\mathbf{x}}$ when the forward model is called to calculate a radiance:

$$\hat{\mathbf{x}} = \mathbf{M}\hat{\mathbf{z}} \qquad (3)$$

The matrix **M** performs a piecewise linear interpolation by log pressure from the lower number of layers in $\hat{\mathbf{z}}$ to the higher number of layers in $\hat{\mathbf{x}}$.

T_{atm}, T_{surf}, and T_{cldtop} are linear quantities in the state vector. Logarithmic quantities for H_2O, O_3, CO_2, τ_{cld}, and r_{eff} are used in the state vector to ensure that their linear values always remain positive when input to the forward model during retrieval iterations. For land surface emissivity (ε_{surf}), a variant of the logistic function (described below in Sec. 2.2.7) is used in order to restrict the forward model emissivity to be between 0 and 1. The state vector thus usually contains linear, logarithmic and (over land) logistic function elements. Description and determination of the different elements of the cost function are described in the sections below.

Layer# (0 offset)	Pressure (mb)	Retrieval layer for …			
0	0.009	T_{atm}	H_2O	CO_2	O_3
1	0.026				
2	0.055				
3	0.104				
4	0.177				
5	0.281				
6	0.421	T_{atm}			O_3
7	0.604				
8	0.838				
9	1.129				
10	1.484	T_{atm}			
11	1.910				
12	2.416				
13	3.009				
14	3.696	T_{atm}			O_3
15	4.485				
16	5.385				
17	6.402				
18	7.545	T_{atm}			
19	8.822				
20	10.240				
21	11.807				
22	13.532	T_{atm}		CO_2	O_3
23	15.423				
24	17.486				
25	19.730				
26	22.163	T_{atm}			
27	24.793				
28	27.626				
29	30.671	T_{atm}	H_2O		O_3
30	33.934				
31	37.425				
32	41.148				
33	45.113				
34	49.326	T_{atm}			O_3
35	53.794				
36	58.524				
37	63.523				
38	68.797				
39	74.353	T_{atm}	H_2O	CO_2	O_3
40	80.198				
41	86.338				
42	92.778	T_{atm}			
43	99.526				
44	106.586	T_{atm}	H_2O		O_3
45	113.965				
46	121.669	T_{atm}			
47	129.703				
48	138.071	T_{atm}	H_2O		O_3
49	146.781				

Layer# (0 offset)	Pressure (mb)	Retrieval layer for …			
50	155.836	T_{atm}			
51	165.241				
52	175.001	T_{atm}	H_2O	CO_2	
53	185.122				
54	195.606	T_{atm}			O_3
55	206.459				
56	217.685	T_{atm}	H_2O		
57	229.287				
58	241.270	T_{atm}			O_3
59	253.637				
60	266.392	T_{atm}	H_2O		
61	279.537				
62	293.077	T_{atm}			O_3
63	307.014				
64	321.351	T_{atm}	H_2O	CO_2	
65	336.091				
66	351.236	T_{atm}			O_3
67	366.789				
68	382.751	T_{atm}	H_2O		
69	399.126				
70	415.914	T_{atm}			O_3
71	433.118				
72	450.738	T_{atm}	H_2O		
73	468.777				
74	487.236	T_{atm}			O_3
75	506.115				
76	525.416	T_{atm}	H_2O		
77	545.139				
78	565.285	T_{atm}		CO_2	
79	585.854				
80	606.847	T_{atm}	H_2O		
81	628.263				
82	650.104	T_{atm}			O_3
83	672.367				
84	695.053	T_{atm}	H_2O		
85	718.162				
86	741.693	T_{atm}	H_2O	CO_2	
87	765.645	T_{atm}	H_2O		
88	790.017	T_{atm}	H_2O		
89	814.807	T_{atm}	H_2O		
90	840.016	T_{atm}	H_2O		O_3
91	865.640	T_{atm}	H_2O		
92	891.679	T_{atm}	H_2O	CO_2	
93	918.130	T_{atm}	H_2O		
94	944.993	T_{atm}	H_2O		
95	972.264	T_{atm}	H_2O		
96	999.942	T_{atm}	H_2O	CO_2	
97	1028.025	T_{atm}	H_2O		
98	1056.510	T_{atm}	H_2O		
99	1085.394	T_{atm}	H_2O	CO_2	O_3

Table 1: Forward model layer pressures and retrieval pressures for constituents.

2.2 A priori profiles, scalars and vectors

2.2.1 Temperature profile, water vapor, surface temperature, and ozone

Initial guess profiles for T_{atm}, H_2O, T_{surf}, and surface pressure (P_{surf}, the latter remaining fixed during the retrieval) are derived from NCEP forecast data, at 1° and 6-hour resolution, linearly interpolated in time and space to that of the observed footprint, with vertical profiles linearly interpolated by the logarithm of the retrieval pressure layering. (For consistency's sake, we have kept the 1° and 6-hour resolution throughout the mission, despite higher forecast resolutions becoming available.) Above the vertical limit of NCEP forecasts, a climatology for temperature and water vapor derived from the Upper Atmosphere Research Satellite (UARS) was used, similar to that used for the AIRS V4 "cloud-cleared" retrieval (Barnet et al., 2007, Sec. 3.4). Initial O_3 profiles are calculated from the climatology of McPeters et al. (2007).

2.2.2 Carbon dioxide

A priori CO_2 profiles are calculated by formulae developed by G. C. Toon (personal communication), and are similar to those used by the Total Carbon Column Observing Network (Wunch et al., 2011).

The reference CO_2 volume mixing ratio is assumed to be 380 ppmv at the start of calendar year 2005 with a 0.5% rate of yearly increase. Thus, for a given day in a given year,

$$CO_{2,\,ref} = 0.000380 * (1. + R*(\text{year} + \text{DOY}/365.25 - 2005.)) \quad (4)$$

where:

$CO_{2,ref}$ is the reference CO_2,
R is the yearly fractional increase in CO_2 abundance (0.005),
DOY is the ordinal date (i.e., January 1 = 1, February 1 = 32, etc.), and
year is calendar year.

The planetary boundary layer pressure (in atmospheres) is calculated as

$$P_{PBL} = 0.70 - 0.15 * \cos(4 * \pi * \text{lat}/360) - 0.1 * \sin(2 * \pi * \text{lat}/360) * \sin(2 * \pi * (\text{dayOfYear} - 110)/365.25) \quad (5)$$

with the result multiplied by 1013.25 to produce an answer in millibar.

The tropopause pressure is assumed from the latitude (in degrees), and varies from 90 hPa in the tropics to 280 hPa in the polar regions:

$$P_{trop} = 0.28 - 0.19 * \exp(-((\text{latitude} - \text{sslat})/35.)^2) \quad (6)$$

with sslat being a seasonal modification to the "effective" latitude:

$$\text{sslat} = 12 * \sin(2.*\pi * (\text{DOY} - 120)/365.25) \quad (7)$$

Again, the result is multiplied by 1013.25 to produce an answer in millibar.

The age of the air (in years) is assumed at different regions of the atmosphere:

A_{pbl} = age at the planetary boundary layer = 0.2
A_{trop} = age at the tropopause = 0.4
A_{toa} = age at the top of the model atmosphere = 5.5

if $P_{layer} > P_{PBL}$ (within the planetary boundary layer):

$$\text{age} = \text{apbl} * (P_{surf} - P_{layer})/(P_{surf} - P_{PBL}) \quad (8)$$

else if $P_{layer} > P_{trop}$ and $P_{layer} < P_{PBL}$ (in free troposphere):

$$\text{age} = A_{pbl} + (A_{trop} - A_{pbl}) * (P_{PBL} - P_{layer}) / (P_{PBL} - P_{trop}) \quad (9)$$

else if $P_{layer} <= P_{trop}$ (in stratosphere or higher):

$$\text{age} = A_{toa} - (A_{toa} - A_{trop}) * \text{sqrt}(P_{layer} /P_{trop}) \quad (10)$$

The intial volume mixing ratio of CO_2 is set at a model layer:

$$vmr_0 = CO_{2,ref} * (1. - R * \text{age}) \quad (11)$$

The fractional amplitude of the seasonal cycle at the surface is calculated as:

$$fasc = 0.01 * \sin(2. * \text{lat} * (1 - \text{lat}/720.) * \pi / 180.) * \exp(\text{lat} / 45.) \quad (12)$$

A seasonal correction is applied depending on the day of the year and age of air:

$$x = \sin(2. * \pi * (\text{dayOfYear} + 75.)/365.2 - \text{age})$$

$$\text{sdma} = 1.45 - \exp(-1.11*x) \quad (13)$$

The a priori CO_2 volume mixing at a model layer is finally calculated as:

$$CO_2 = vmr_0 * (1 + fasc * \exp(-\text{age}/0.25) * \text{sdma}) \quad (14)$$

2.2.3 MODIS cloud a priori information and mapping to AIRS footprint

For a priori data on cloud-top temperature (T_{cldtop}), cloud optical depth (τ_{cld}) and effective cloud particle radius (r_{eff}) in each AIRS observation, weighted averages of MODIS Level 2 T_{cldtop}, cloud emissivity (ε_{cld}) and (during daytime) r_{eff} data are made over the AIRS spatial response function (SpatialRF) using the algorithm of Wang et al. (2016). Cloud optical depth is calculated from the cloud emissivity (ε_{cld}). (See Sect. 2.25 below.) A pre-computed average AIRS SpatialRF (using all AIRS channels) is used in weighting the MODIS pixels to the AIRS footprint (see Schreier et al., 2010, and Pagano et al., 2015); this average varies by AIRS scan angle and MODIS along-track and cross-track pixels. MODIS data from the MYD06_L2 (Aqua) product (with a horizontal resolution of about 1 km at nadir) are then mapped in the vicinity of the AIRS observation.

Once the AIRS and MODIS footprints are co-located, MODIS retrieval fields for cloud-top temperature, cloud emissivity, and cloud effective radius are extracted and mapped (as data are available). Weighted averages and weighted standard deviations of the MODIS T_{cldtop} and r_{eff} are then calculated on the interpolated AIRS SpatialRF, excluding MODIS cloud-free pixels, while MODIS cloud emissivities are averaged where the data are greater or equal to zero. From the MODIS Cloud_Mask_1km field, we extract, map and similarly weight the cloud mask status (0 = undetermined, 1 = determined), cloud mask cloudiness (0 = confidently cloudy or fill if status flag = 0, 1 = probably cloudy, 2 = probably clear, 3 = confidently clear) and thin cirrus flags (0 = yes or fill if status flag = 0, 1 = no).

Additionally, for each observed spectrum, we calculate "Cloud Phase Scores" as described by Kahn et al. (2014). The "Ice_cloud_total_score" and "Liquid_cloud_total_score" are calculated using brightness temperatures (T_b) of specific AIRS channels (see **INSET 1**).

2.2.4 Cloud-top temperature (T_{cldtop})

The weighted averages of the MODIS flags over the AIRS scene are combined with the Cloud Phase Scores, and are used to decide (a) if the scene is clear, (b) a cloud too thin for a confident MODIS retrieval of its cloud-top temperature is in the scene, but retrieval by AIRS should be attempted using an assumed cloud-top temperature a priori, or (c) retrieval in a cloudy scene will be attempted using the averaged MODIS cloud data as a priori. We categorize AIRS scenes as:

(1) Clear,

(2) Cloudy of known MODIS temperature,

(3) Thin cirrus of unknown MODIS temperature,

(4) Liquid cloud of unknown MODIS temperature,

(5) Mixed-phase of unknown MODIS temperature, or

(6) Default cloud of unknown MODIS temperature,

and set a priori cloud data accordingly. We describe the criteria for these bins in turn, and the cloud-top temperature a priori selected for them.

Set:

$T_{b,930}$ = mean(T_b @ 930.07 cm^{-1}, T_b @ 930.44 cm^{-1}, T_b @ 930.81 cm^{-1})
$T_{b,960}$ = mean(T_b @ 960.27 cm^{-1}, T_b @ 0960.66 cm^{-1})
$T_{b,1227}$ = mean(T_b @ 1227.1910 cm^{-1}, T_b @ 1227.71 cm^{-1})
$T_{b,1290}$ = mean(T_b @ 1231.33 cm^{-1}, T_b @ 1231.85 cm^{-1})

where T_b is the brightness temperature (in K).

(Ice cloud tests)

Set Ice_cloud_total_score = 0

if $T_{b,960} < 235.0$ K:
    Ice_cloud_total_score += 1
if $(T_{b,1231} - T_{b,960}) > 0$ K:
    Ice_cloud_total_score += 1
if $(T_{b,1231} - T_{b,930}) > 1.75$ K:
    Ice_cloud_total_score += 1
if $(T_{b,1227} - T_{b,960}) > -0.5$ K:
    Ice_cloud_total_score += 1

(Liquid cloud tests)

Set Liquid_cloud_total_score = 0

if $(T_{b,1231} - T_{b,960}) < -1$ K:
    Liquid_cloud_total_score −= 1
if (Tb_1231 - Tb_930) < -0.6 K:
    Liquid_cloud_total_score −= 1

INSET 1: Procedure for determining cloud phase scores. The wavenumbers shown are approximate as the centroid of the channel frequency response, and can change with shifting by the AIRS focal plane during the course of the mission.

2.2.4.1 Clear

An AIRS scene is treated as clear if

(a) the average for the Cloud Mask Status Flag is greater than 0.95, and

(b) the average Cloud Mask Cloudiness is greater than 2.8, and

(c) Ice_cloud_total_score and Liquid_cloud_total_score are both zero, and

(d) (during daytime) the average Thin Cirrus Flag is greater than 0.95.

In this case, no cloud information is in the retrieval or full state vector, and the retrieval algorithm goes directly to retrieve T_{atm}, T_{surf}, H_2O, O_3, CO_2 and (over land) emissivity

2.2.4.2 Cloudy of known MODIS temperature

A scene is treated as cloudy (ice or water cloud) if the weighted average of the MODIS cloud-top temperature on the AIRS footprint can be calculated. The result is used as the a priori T_{cldtop}.

2.2.4.3 Thin cirrus of unknown MODIS temperature

A scene is considered to have thin cirrus but of unknown temperature if

(a) the cloud-top temperature cannot be calculated because of missing MODIS values, and
(b) the Ice_cloud_total_score > 0, and
(c) the Liquid_cloud_total_score = 0.

OR

(a) the solar zenith angle is below 85° (daytime), and

(b) the Ice_cloud_total_score = 0, and

(c) the Liquid_cloud_total_score = 0, and

(d) the averaged MODIS thin cirrus flag < 0.9.

In this case, we assume a default a priori T_{cldtop} of 230K, except if this is within 10K of the a priori surface temperature. If the latter is true, then the a priori cloud-top temperature is set to the a priori surface temperature minus 10K.

2.2.4.4 Liquid cloud of unknown MODIS temperature

A scene is considered to have a liquid cloud but of unknown temperature if

(a) the cloud-top temperature cannot be calculated because of missing MODIS values, and
(b) the Ice_cloud_total_score = 0, and
(c) the Liquid_cloud_total_score < 0.

In this case, we assume a default a priori T_{cldtop} of 280K, except if this is within 10K of the a priori surface temperature, in which case the a priori cloud-top temperature is set to the a priori surface temperature minus 10K.

2.2.4.5 Mixed-phase cloud of unknown MODIS temperature

A scene is considered to have a mixed-phase cloud but of unknown temperature if

(a) the cloud-top temperature cannot be calculated because of missing MODIS values, and
(b) the Ice_cloud_total_score > 0, and
(c) the Liquid_cloud_total_score < 0.

In this case, we assume a default a priori T_{cldtop} of 270K, except if this is within 10K of the a priori surface temperature, in which case the a priori cloud-top temperature is set to the a priori surface temperature minus 10K.

2.2.4.6 Default cloud of unknown MODIS temperature

A scene is considered to have a cloud of unknown phase and temperature if

(a) the cloud-top temperature cannot be calculated because of missing MODIS values, and

(b) the Ice_cloud_total_score is 0, and

(c) the Liquid_cloud_total_score is 0, and

(d) the scene does not pass either the "*Clear*" criteria (Sec. 2.2.4.1) or the "*Thin cirrus of unknown temperature"* (Sec. 2.2.4.3) as described above.

In this case, we assume a default a priori T_{cldtop} of 240K, except if this is within 10K of the a priori surface temperature, in which case the a priori cloud-top temperature is set to the a priori surface temperature minus 10K.

2.2.5 Cloud optical depth (τ_{cld})

If the scene is *not* clear as determined by the test described in Sec 2.2.4.1 above, then the a priori cloud optical depth is calculated from an averaged MODIS cloud emissivity (ε_{cld}).

$$\tau_{cld} = -2. * \ln(1. - \varepsilon_{cld}) \quad (15)$$

If ε_{cld} is less than 0.01, it is reset to 0.01. If ε_{cld} is greater than 0.99, it is reset to 0.99. We note that in this formulation, the a priori τ_{cld} cannot be less than 0.02 nor greater than 9.21. If the averaged MODIS cloud emissivity cannot be calculated because of missing values, then ε_{cld} is assumed to be 0.05, giving an a priori τ_{cld} of 0.12.

2.2.6 Cloud effective particle radius (r_{eff})

If the weighted average of the MODIS r_{eff} can be calculated, it is used as the a priori. If the average cannot be calculated, or if it is nighttime, the default r_{eff} is 40 μm. Lookup tables for cloud absorption and scattering parameters have particle radii ranging from 5 to 85 μm; reported cloud absorption and scattering parameters outside this range rely on extrapolated parameters, and results may not be reliable.

2.2.7 Land emissivity (ε_{surf})

For ocean emissivity, we use the National Center for Environmental Prediction – Environmental Modeling Center (NCEP/EMC) Infrared Sea Surface Emissivity (IRSSE) formulae and coefficients (van Delst, 2003), calculated for channel frequency, view angle and wind speed, with the latter estimated from the NCEP forecast (described above). Channel-dependent ocean emissivities are input as fixed parameters, and are not retrieved or modified.

Over land or mixed land-ocean surfaces, emissivity is from the Cooperative Institute for Meteorological Satellite Studies, University of Wisconsin - Madison Global Infrared Land Surface Emissivity Database (Seemann et al., 2008). These are monthly maps of land emissivity at 10 wavelengths from 3.6 to 14.3 μm, gridded spatially by 0.05°. Emissivities are spatially interpolated to the center of the coincident AIRS footprint. If missing values are in the emissivity database at locations used for interpolation to the center of the AIRS footprint, they are assumed to be ocean, with ocean emissivities calculated as above. Emissivities for each AIRS retrieval channel are then calculated by interpolation by wavelength. As the emissivity database does not extend prior to calendar year 2003 or past 2014, we use a data set averaged on a month-by-month basis for those years where specific data are unavailable.

We do not retrieve land emissivities in linear space since it's possible that the optimal estimation algorithm could crash the forward model by testing emissivities less than zero or greater than unity. To avoid this, we use a variant of the logistic function to restrict the emissivity to be between 0 and 1:

$$\varepsilon_{surf} = \frac{L}{1+\exp\left(-k[\xi-\xi^*]\right)} \tag{16}$$

The emissivity is converted to logistic space by inverting Eq. 16. We select L = 1, k = 1 and ξ^* = 5. Thus, the "logistic parameter" function becomes:

$$\xi = 5 - ln\left(\frac{1}{\varepsilon_{surf}} - 1\right) \tag{17}$$

Within the retrieval, we solve for ξ, converting back to ε_{surf} via Eq. 16 when emissivity is input into the forward model. The value for ξ is initialized from the a priori ε_{surf}.

Within the spectral range of the JoSFRA retrieval, we retrieve emissivities using hinge points at 699.3, 826.4, 925.9., 1075.2, 1204.8, and 1315.7 cm^{-1}, with interpolations by wavelength (not frequency) for use within the forward model between the 699.3 and 1315.7 cm^{-1} endpoints. Outside this range, endpoints are used. (That is, for frequencies less than 699.3 cm^{-1}, the emissivity at 699.3 cm^{-1} is used, while the emissivity at 1315.7 cm^{-1} is used at frequencies greater than 1315.7 cm^{-1}.) Note that the retrieval need not use AIRS channels corresponding to

the hinge points; the hinge point frequencies are just a basis on which to interpolate the emissivity to the retrieval channels.

2.3 A priori and measurement covariances

2.3.1 A priori covariances

A priori covariances ($\mathbf{S}_a$ in Eq. 1) are listed in Table 2. The covariances are ad hoc, but guided by previous experience with AIRS and TES retrievals. We recommend caution in applying resultant errors, although they may still be useful in comparing results between retrievals. Note that H_2O, O_3, CO_2, τ_{cld} and r_{eff} are retrieved as $\log_e$ quantities, and the covariances of their logarithms are used.

Constituent	Sqrt(covariance) along diagonal	Covariance off-diagonal length scale (km)
Temperature profile (T_{atm})	2K from surface to 50 mb, then gradually increasing to 15K at 10 mb and above.	0.5
Surface temperature (T_{surf})	2K	n/a
H_2O	$\log_e(1.4)$ from surface to 100 mb then gradually reduced to $\log_e(1.01)$ at 50 mb and above	0.5
O_3	$\log_e$ (1.1) from ground to 100 mb then gradually increasing to $\log_e$ (1.2) at 50 mb and above	3.0
CO_2	$\log_e(1.02)$	3.5
Cloud optical depth (τ_{cld})	$\log_e(2)$	n/a
Cloud-top temperature (T_{cldtop})	4K (see text)	n/a
Cloud particle radius (r_{cld})	$\log_e(2)$	n/a
Land emissivity parameter ξ (see Sec. 2.2.7)	Varies (see Sec 2.3 text)	n/a
Surface pressure (P_{surf}; not retrieved, but used in error calculation)	2 mb	n/a

n/a = not applicable.

Table 2: A priori covariances and off-diagonal length scale.

A relaxed covariance for T_{atm} is used at the lowest forward model pressures ($\lesssim$ 50 hPa) since the vertical extrapolation from the NCEP forecast can produce significant temperature bias under the extremely cold conditions sometimes seen in the polar upper stratosphere or lower mesosphere. A $(2K)^2$ a priori covariance can be too constraining to allow a good spectral fit for the retrieval, so the covariance increases from $(2K)^2$ at 50 hPa to $(15K)^2$ at 10 hPa and above.

As noted, emissivity over land is not retrieved in linear space. Instead, the logistic parameter ξ is retrieved from which the emissivity is calculated (Eq. 16). The a priori covariance for ξ was

derived at each grid point and hinge frequency by calculating the monthly average and covariance (across hinge frequencies) of ξ from 2003 through 2014 using the Seemann et al. (2008) data. From these data, the variance of ξ at a hinge frequency at the AIRS observation is interpolated if possible. If a variance is not available, a value of 0.26 is assumed. Only the diagonal of the ξ covariance matrix is used; no off-diagonal components (e.g., across different hinge points) are used.

For temperature and gas retrievals, off-diagonal elements of the covariance matrices are created using assumed length scales:

$$\sigma_{ij}^2 = \sigma_i \sigma_j \exp\left(-\frac{|z_i - z_j|}{l}\right) \tag{18}$$

where:

σ_{ij}^2 is the off-diagonal covariance for layers *i* and *j*,
σ_i, σ_j are the square roots of the on-diagonal covariances,
z_i, z_j are the estimated altitudes, and
l is the assumed length scale.

The off-diagonal length scale for temperature and water vapor was kept low (0.5 km) as this tended to reduce unrealistic retrievals at layers below thick clouds from adversely affecting retrievals above clouds. (This is discussed further in Sect. 2.4 below.) Covariance matrices are calculated individually for each constituent and then "stacked" into a larger matrix for use in the simultaneous retrieval. At present, we are not using covariances between constituents (say, between temperature and water vapor.)

2.3.2 Note on cloud-top temperature a priori covariance

After routine processing began, a programming error was discovered in that an incorrect a priori covariance for the cloud-top temperature (T_{cldtop}) was used when the cloud-top temperature a priori was assumed and not derived from MODIS (see Sec. 2.2.4). In these cases, the a priori covariance for a MODIS-derived cloud-top temperature, $(4K)^2$, was erroneously used when a covariance of $(25K)^2$ should instead have been used. The resulting T_{cldtop} retrieval in cases where the a priori T_{cldtop} was assumed may thus be overly-close to the first guess, and is likely to have an underestimated error. This will be corrected in future versions of JoSFRA. The full effect of

this error needs to be evaluated, however, we anticipate such cases tend to occur under low cloud opacity, and this is not expected to significantly affect retrievals of other parameters.

2.3.3 Measurement error covariance

Measurement error covariance ($\mathbf{S}_\varepsilon$ in Eq. 1) is taken directly from the radiometric noise reported in the AIRS Level 1b product (see Pagano et al., 2003). This is reported channel-by-channel, without correlations between them. For this study, $\mathbf{S}_\varepsilon$ is a diagonal matrix, and we have assumed the noise to be uncorrelated across channels, Gaussian, and not scene-dependent. A study by Tobin et al. (2007), using Principal Component Analysis on AIRS radiance data, showed the contribution from correlated error can be significant depending on the detector array on the AIRS focal plane. (See also Pagano, 2002.) Channel radiance error can be dependent on the channel radiance in the shortwave above ~2200 cm^{-1}, but these channels are not used in this study. Only a minor dependence of the radiance error on channel radiance is observed in the midwave (~1200 to 1700 cm^{-1}) and there is effectively no dependence for channels below ~1200 cm^{-1}. Individual channels sometimes exhibit non-Gaussian "popping", that is, a transitory step change in the signal noted during the instrument's deep space and on-board calibration views (see Weiler et al., 2005). These channels are excluded from analysis of an observation.

Random errors in the calculated radiances from the forward model (briefly described below in Sec. 2.4) are not added into the measurement error covariance as used in this algorithm. The random errors from the "non-cloudy" part of forward model may be smaller than the noise error from the AIRS instrument for most channels (see, for example, Fig. 2 in DeSouza-Machado et al., 2018), but significant random error may be introduced from the calculation of the cloud absorption and emission.

2.4 Forward model

The forward model is the Standalone AIRS Radiative Transfer Algorithm (SARTA) (Strow et al., 2003; 2006), supplemented with a delta-four-stream (D4S) calculation for cloud transmissivity (Ou et al., 2013). For ice clouds, scattering parameters are from Baum et al. (2007). For water clouds, we use Mie scattering parameters calculated using formulae from Mishchenko et al. (2002). Only cirrus parameters are used at cloud-top temperatures (T_{cldtop})

below 253.15 K, while only Mie cloud parameters are used at temperatures above 273.15 K. Between these temperatures, we use a sliding weight between Mie and cirrus-derived cloud.

Within the SARTA+D4S forward model, SARTA calculates the cloud-free gaseous transmissivities for each pressure layer and retrieval channel given the temperature and gas profiles, emissivity, scan angle, etc. The D4S code calculates the cloud transmissivities for retrieval channels given a cloud-top temperature, optical depth and particle size. To find the correct model layer in which to put the cloud, the code tests the layer temperatures downwards from ~100mb until it finds a layer where the temperature is greater or equal to the cloud-top temperature. Given the cloud-top temperature, the cloud-top pressure is then calculated by linear interpolation of the natural logarithm of the layer pressures with the layer temperatures. The cloud layer is determined where the cloud-top pressure is between forward model *level* pressures. (See Fig. 5.) Each pressure layer in the forward model is assumed homogeneous for gases, however, the "cloudy" layer is subdivided into clear and cloudy sublayers. The fraction of a (full) layer that is cloudy (*f*) is effectively determined as the weight fraction of the gas in the cloudy part of the layer. (Note that the layer indices are ordered downward from the top of the atmosphere):

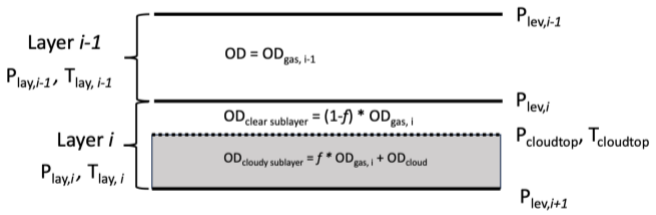

Figure 5: Schematic of forward model clear and cloudy layers. P is pressure, T is temperature, and *f* is the fraction of a model layer that is cloudy. Layer numbers are indexed from top-of-atmosphere downwards. Note that OD_{cloud} is the infrared optical depth of the cloud specific to an AIRS channel frequency, and is not the visible optical depth reported in the retrieval output.

$$f = \frac{P_{cloudtop} - P_{lev,i}}{P_{lev,i+1} - P_{lev,i}} \qquad (19)$$

The optical depth of the gases in the cloudy layer is fractionally divided between the clear and cloudy sublayers, with the (channel specific) optical depth of the cloud (calculated from the transmissivity) added to the gas optical depth of the cloudy sublayer. Here, the upwelling and downwelling radiance calculation is also calculated at the cloud-top pressure, in addition to the normal calculation at layer pressure boundaries.

Note that this models the cloud as "fitting" in one forward-model sublayer, no matter how thick the cloud. Indeed, the cloud becomes infinitely thin if a cloud-top pressure falls exactly on a level pressure (but the cloud transmittance is still used in calculating the outgoing radiance.) This forward modelling of temperature, trace gases and cloud properties, while computationally fast, is best suited for optically and geometrically thin clouds, and may not be well suited for thick clouds, or where significant cloud formations occupy different heights within an AIRS pixel. These scenes often, but not always produce retrievals with poor spectral fits (described below in Sec. 2.7.4) and are filtered out in quality control. "Distribution" of a cloud transmissivity over several model layers will be investigated and perhaps incorporated into future versions of JoSFRA.

2.5 Retrieval channels

Table 3 lists the spectral channels used in JoSFRA retrievals. Only longwave channels were used (< 1650 cm^{-1}). We found that using channels in the shortwave region of the AIRS bandpass would often result in retrievals not converging, or producing unrealistic retrieval quantities.

2.6 Retrieval by minimization of cost function

After setting the different elements of the cost function (Eq. 1) as described above, the retrieval is performed by iteratively minimizing the cost function by modifying the retrieval state vector $\hat{\mathbf{z}}$ with a combination Gauss-Newton/Levenberg-Marquardt solver. Formulae are described by Bowman et al. (2006), applying the algorithm of Moré (1977). (See also Sarkissian, 2001.)

A simultaneous retrieval of τ_{cld}, T_{cldtop}, r_{eff}, T_{surf}, T_{atm}, H_2O, O_3, CO_2 and (over land) ε_{surf} is made. Convergence tests are as described in Sect. IV.B(2) of Bowman et al. (2006), setting the threshold value ("ε") of 0.2. If a given retrieval cannot converge within a specified number of iterations, or both the level 2 norm of the trust region ("Δ" in Moré, 1997) and linearity measure ("ρ") within the Levenberg-Marquardt solver fall below 10^{-3}, the algorithm is stopped and

flagged as non-convergent. Converged retrievals are analysed for information content and quality-control (QC) checked as described below.

Step One Channels							
Channel (zero offset)	Approx. Frequency (cm^{-1})	Channel (zero offset)	Approx. Frequency (cm^{-1})	Channel (zero offset)	Approx. Frequency (cm^{-1})	Channel (zero offset)	Approx. Frequency (cm^{-1})
51	662.02	*154*	694.12	*240*	718.58	*432*	779.11
61	664.51	*155*	694.40	*241*	718.87	*444*	790.33
68	666.26	*156*	694.67	*242*	719.17	*454*	793.89
70	666.77	*160*	695.77	*243*	719.46	*468*	798.92
72	667.27	*161*	696.05	*244*	719.76	*474*	801.10
74	667.78	*166*	697.43	*248*	720.94	*481*	803.65
76	668.28	*167*	697.71	*250*	721.54	*484*	804.75
77	668.54	*171*	698.82	*251*	721.83	*503*	811.79
78	668.79	*172*	699.10	*255*	723.03	*527*	820.84
79	669.04	*173*	699.38	*256*	723.32	*576*	839.92
81	669.55	*174*	699.66	*260*	724.52	*594*	847.14
82	669.81	*178*	700.77	*266*	726.32	*600*	849.57
83	670.06	*179*	701.05	*294*	734.15	*699*	880.40
85	670.57	*185*	702.74	*308*	738.48	*786*	917.30
91	672.10	*189*	703.87	*313*	740.03	*842*	937.90
97	673.64	*191*	704.43	*332*	746.01	*1240*	1125.27
103	675.19	*197*	706.13	*337*	747.60	*1241*	1125.81
109	676.75	*200*	706.99	*342*	749.20	*1242*	1126.35
110	677.01	*203*	707.84	*346*	750.48	*1243*	1126.89
115	678.31	*206*	708.70	*351*	752.09	*1244*	1127.42
116	678.57	*209*	709.56	*355*	753.38	*1245*	1127.96
127	681.46	*214*	711.00	*356*	753.70	*1246*	1128.50
128	681.72	*215*	711.29	*360*	755.00	*1247*	1129.04
137	689.49	*220*	712.74	*361*	755.32	*1248*	1129.58
138	689.76	*225*	714.19	*370*	758.26	*1249*	1130.12
143	691.12	*226*	714.48	*405*	769.89	*1250*	1130.66
144	691.39	*231*	715.94	*415*	773.28	*1290*	1231.33
149	692.75	*238*	717.99	*424*	776.36	*1291*	1231.85
150	693.02	*239*	718.28	*429*	778.08	*1292*	1232.37
Step Two Channels							
Channel (zero offset)	Approx. Frequency (cm^{-1})	Channel (zero offset)	Approx. Frequency (cm^{-1})	Channel (zero offset)	Approx. Frequency (cm^{-1})	Channel (zero offset)	Approx. Frequency (cm^{-1})
402	768.88	*1265*	1218.49	*1592*	1407.77	*1739*	1513.83
405	769.89	*1278*	1225.13	*1626*	1427.22	*1744*	1517.10
459	795.68	*1413*	1310.18	*1635*	1432.47	*1769*	1547.20
493	808.07	*1422*	1315.47	*1651*	1441.88	*1775*	1551.30
509	814.03	*1518*	1367.25	*1657*	1462.09	*1805*	1572.09
538	825.05	*1536*	1376.88	*1668*	1468.82	*1825*	1586.26
545	827.75	*1544*	1381.21	*1685*	1479.36	*1834*	1592.72
869	948.18	*1550*	1384.47	*1692*	1483.74	*1842*	1598.50
1232	1121.00	*1564*	1392.15	*1707*	1493.21	*1851*	1605.05
1259	1135.55	*1573*	1397.13	*1721*	1502.16		

Table 3: AIRS channels and approximate frequencies for Step One and Step Two Retrievals.

2.7 Information content and error estimation

2.7.1 Averaging kernels

Averaging kernels (see Chapter 2.4 in Rodgers, 2000) are internally calculated within JoSFRA, but are not routinely output. We assume that the retrieval is nearly linear in the vicinity of the solutions. The Jacobian is defined as the matrix of derivatives of the outgoing radiance to changes in each element of the state vector,

$$\mathbf{K}_{\mathrm{z}} = \frac{\partial \mathbf{F}(\hat{\mathbf{x}}, \mathbf{b})}{\partial \mathbf{z}} = \frac{\partial \mathbf{F}(\mathbf{M}\hat{\mathbf{z}}, \mathbf{b})}{\partial \mathbf{z}} \tag{20}$$

and is calculated by finite difference for each retrieval iteration. The gain, $\mathbf{G}_z$, is a measure of the sensitivity of the retrieval, $\hat{\mathbf{z}}$, to changes in the radiance:

$$\mathbf{G}_z = \frac{\partial \hat{\mathbf{z}}}{\partial \mathbf{F}} = (\mathbf{K}_z^T \mathbf{S}_\varepsilon^{-1} \mathbf{K}_z + \mathbf{S}_a^{-1})^{-1} \mathbf{K}_z^T \mathbf{S}_\varepsilon^{-1} \tag{21}$$

The gain is multiplied by the Jacobian to produce the averaging kernel matrix, **A**, which is a measure of the sensitivity of the retrieval vector, $\hat{\mathbf{z}}$, to changes in the true state, **z**:

$$\mathbf{A} = \frac{\partial \hat{\mathbf{z}}}{\partial \mathbf{z}} = \frac{\partial \hat{\mathbf{z}}}{\partial \mathbf{F}} \frac{\partial \mathbf{F}}{\partial \mathbf{z}} = (\mathbf{K}_z^T \mathbf{S}_\epsilon^{-1} \mathbf{K}_z + \mathbf{S}_a^{-1})^{-1} \mathbf{K}_z^T \mathbf{S}_\epsilon^{-1} \mathbf{K}_z \tag{22}$$

This is a square matrix dimensioned $n \times n$, where n is the number of elements of the state vector, and as described below, is useful in calculating the error covariance of the retrieval. Each element of the averaging kernel matrix is a measure of the sensitivity for one retrieved member of a state vector $(\hat{\mathrm{z}}_i)$ to the changes in the true value of that member (z_i), or to the true value of a different member (z_j). That is,

$$\mathrm{A}_{i,j} = \frac{\partial \hat{\mathrm{z}}_i}{\partial \mathrm{z}_j} \tag{23}$$

Note for an AIRS retrieval, an averaging kernel is scene dependent. Sensitivities at different layers depend on the amounts of trace gases present, the temperature lapse rate, the particulars of the cloud field, the view angle, and the spectral channels employed. Since the JoSFRA (Step One) retrievals are simultaneous and not sequential, the averaging kernel describes dependencies within and between retrievals of different constituents, and can be used to more robustly calculate uncertainties as described below.

While the full averaging kernels are not routinely output, the averaging kernel (Eq. 22) itself is subset for individual retrieval constituents, and the traces of these submatrices are output as Degrees of Freedom of Signal (DOFS.) The DOFS is a measure of the number of independent pieces of information retrieved from the measurement of a constituent. This is more fully described in Sec 2.4.2 of Rodgers, 2000, but we note here that the DOFS for surface temperature is used in quality control for retrievals in cloudy conditions (Sec 2.8 below.)

2.7.2 Error estimation

The smoothing error covariance measures the uncertainty in the fine structure of the retrieval due to the measurement's limited vertical resolution. However, as we have an averaging kernel from a joint retrieval, the smoothing error also indicates how the uncertainty in one retrieved constituent affects the uncertainty in another:

$$\mathbf{S}_s = (\mathbf{A} - \mathbf{I}_\mathrm{n})\mathbf{S}_a(\mathbf{A} - \mathbf{I}_\mathrm{n})^T \tag{24}$$

(See Sect. V(B) of Bowman et al., 2006, and Sections 3.4 and 4.1 of Rodgers, 2000.)

The retrieval noise error covariance calculates the impact of the radiance noise on the retrieval:

$$\mathbf{S}_\mathrm{m} = \mathbf{G}_z\mathbf{S}_\varepsilon\mathbf{G}_z^T \tag{25}$$

With substitutions, these terms can be added to provide the covariance of the maximum a posteriori solution:

$$\hat{\mathbf{S}} = (\mathbf{K}_z^T\mathbf{S}_\varepsilon^{-1}\mathbf{K}_z + \mathbf{S}_a^{-1})^{-1} \tag{26}$$

with the square roots of the diagonal reported as errors for the state vector. Note also that the total retrieval error does not include any systematic errors from the forward model (e.g., those due to instrumental lineshape errors, spectral biases or other errors that are correlated across observations), although we note the SARTA model is "tuned" to better match outgoing radiances as calculated from coincident measurements and analyses (see Strow et al., 2006). We again emphasize that since our a priori covariances are ad hoc, caution should be observed in using the reported errors.

The model parameter error contains the uncertainty from parameters affecting the retrieval, but are not retrieved themselves (e.g., surface pressure, ocean emissivity, scan angle, etc.):

$$\mathbf{S}_{\text{mp}} = \mathbf{G}_{\text{z}}\mathbf{K}_{\text{Psurf}}\mathbf{S}_{\text{a,Psurf}}(\mathbf{G}_{\text{z}}\mathbf{K}_{\text{Psurf}})^{T} + \cdots \tag{27}$$

For this version of JoSFRA, model parameter error is calculated for Step One using an assumed covariance for P_{surf} only, but for the Step Two H_2O retrieval, the model parameter error is calculated using a priori covariances for P_{surf}, T_{atm}, CO_2, T_{cld}, σ_{cld} and r_{cld}, but not O_3 or ε_{surf} over land or water. Using a priori covariances likely results in an overestimate of the model parameter error. Future versions will use a posteriori covariances and will include O_3 or ε_{surf}.

For Step One or Step Two, total retrieval error covariance would be the sum of Eqs. 26 and 27:

$$\mathbf{S}_{\text{tot}} = \hat{\mathbf{S}} + \mathbf{S}_{\text{mp}} \tag{28}$$

Refinement of the model parameter error calculation (Eq. 27) is planned for future development.

For constituents retrieved in logarithmic space, the error reported for the i'th element, ϵ_i, is the error in the logarithm of the retrieved value, $\hat{\mathbf{z}}_i$, with the range [lower, upper] of the retrieval in linear space being:

$$[\exp(\hat{\mathbf{z}}_i - \epsilon_i), \exp(\hat{\mathbf{z}}_i + \epsilon_i)] \tag{29}$$

For errors in the land emissivity (retrieved in logistic space), we apply a simple error calculation heuristic:

$$[df(x)]^2 \approx \left[\frac{df}{dx}\right]^2 [dx]^2 \tag{30}$$

Setting *f* to Eq. 16, *x* to the logistic parameter ξ, *dx* to the square root of the a posteriori covariance of ξ, and making the appropriate substitutions, the emissivity error in the retrieved hinge is calculated as:

$$Error(\varepsilon_{surf}) \approx \frac{\exp(5-\xi)}{[1+\exp(5-\xi)]^2} \times error(\xi) \tag{31}$$

2.7.3 Chi Square Fitting Parameter

The chi square fitting parameter, χ^2, is a goodness-of-fit statistic of how well a spectrum's radiance is fitted within the bounds of the radiance error:

$$\chi^2 = \frac{1}{\mathrm{N}}\sum_{i=1}^{\mathrm{N}}\left(\frac{\mathbf{y}_i - [\mathbf{F}(\mathbf{x},\mathbf{b})]_i}{\varepsilon_i}\right)^2 \quad (32)$$

where N is the number of channels, and ε_i is the radiance error in channel *i*. A $\chi^2 \gg 1$ indicates a poor spectral fit to the observed radiance. While the χ^2 does not directly enter into the error characterization, it is used in quality control as described below.

2.8 Quality control (QC) filtering

There are separate quality control flags for Step One retrievals (T_{atm}, CO_2, O_3, T_{surf}, T_{cldtop}, τ_{cld}, r_{eff}, and ε_{surf}) and Step Two retrievals (H_2O). Flags are 0 (good from top-of-atmosphere to surface), 1 (good from top-of-atmosphere to QCpres, described below), 2 (do not use), and 3 (retrieval failure). We describe the criteria for these in reverse order.

2.8.1 QC = 3 (retrieval failure)

Retrievals that encounter an unrecoverable error in the solver (e.g., attempted inversion of a singular matrix) or elsewhere in the algorithm are given a QC flag = 3 (retrieval failure). No retrieval results or a priori data are written out, although future versions of JoSFRA will write out a priori data.

2.8.2 QC = 2 (do not use)

Retrievals with either or both of the following are output with QC = 2 (Do Not Use):

1. Normal convergence is not obtained within the maximum specified number of iterations (currently 60), or
2. Chi square fitting parameter, $\chi^2 > 3$.

The first criterion is to avoid waste of computational resources on poorly- or non-converging retrievals. The second criterion is to avoid reporting profiles with poor spectral fits. This often

happens under ice cloud conditions when the cloud optical depth is high ($\gtrsim 20$); it's likely that the radiative transfer is incorrectly calculated because a cloud is assumed to "fit" in one vertical model layer while in reality, thick clouds extend over many model layers. Poor spectral fits can also often occur when there was a high standard deviation, $\gtrsim$ 20K, of the MODIS 1 km cloud-top temperature weighted over the AIRS spatial response function. Again, we suspect that this poor fitting is from limitations in our forward model which is limited to one cloud layer; the radiative transfer calculation can be inadequate when there were several cloud tops at different temperatures within the AIRS footprint.

For the users who would prefer to use their own χ^2 criterion in analyzing JoSFRA output, note that the retrieval χ^2's are given in "chi2_step_one" and "chi2_step_two" in the output. Retrievals that have converged normally (regardless of the χ^2) will have "/aux/stop_code_step_one" and/or "/aux/stop_code_step_two" equal to 1. Retrievals that reach the maximum allowable number of iterations will have "/aux/stop_code_step_one" and/or "/aux/stop_code_step_two" equal to 2.

2.8.3 QC = 1 (good from top-of-atmosphere to QCpres)

This QC flag indicates when retrieval profiles are considered good to just above the cloud-top, but are not reliable below. To summarize, retrievals in layers with $T_{atm} > (T_{cldtop} - 10\ K)$ require a surface temperature averaging kernel > 0.6; QCpres is calculated where $T_{atm} = T_{cldtop} - 10\ K$. This is a means to flag layers of a profile that may have unphysical values of the retrieval temperature and/or water vapor below a cloud top.

We again note that a cloud's transmissivity is incorporated in only one layer of the forward model vertical pressure grid, no matter how thick the cloud. We hypothesize that this can lead to erroneous outgoing radiances for temperature and water vapor channels in regions at or below moderately thick clouds, which in turn, produces erroneous Jacobians and averaging kernels. Surface temperature retrievals appear to more correctly give a low-to-zero averaging kernel under moderate-to-thick cloud optical depths. We therefore require that retrievals at layers below clouds must "see" the surface (determined by the T_{surf} averaging kernel having a minimum of 0.6). For retrievals above clouds where the surface temperature averaging kernel is less than 0.6, an additional thermal contrast provided by a 10 K buffer between the cloud top and the lowest

profile layer to pass quality control eliminates more unphysical retrievals. (The 10K buffer was selected by visual inspection of test retrievals, but its size may be revisited in future versions.) Most, but not all of the retrievals that produce unphysically high relative humidities are eliminated by this method, usually in the boundary layer.

2.8.3 QC = 0 (good from top-of-atmosphere to surface)

If a retrieval (a) converges within the specified maximum number of iterations, (b) has a retrieval $\chi^2 \leq 3$, and (c) has a surface temperature averaging kernel > 0.6, then the retrieval is considered "good" from top-of-atmosphere to the surface. (In this case, QCpres is reported as the surface pressure).

Note that it is possible that if the Step One QC flag is 0 or 1, the Step Two QC flag can be 2 (non-convergence or $\chi^2 > 3$) or 3 (retrieval failure). This can happen if the Step Two water vapor retrieval is unsuccessful after a successful Step One retrieval. Note that the QCpres determined in Step One is also used for the Step Two H_2O retrieval profile.

2.9 Calculation of Relative Humidity and Error

In calculating relative humidity (RH), we use the layer retrievals of temperature and water vapor. Eqs. (2.5) and (2.21) of Wagner and Pruß (2002) are used to determine saturation pressures of water vapor over liquid and ice. At temperatures between 253.15 and 273.15K, we set saturation pressure as a sliding-scale weighted average of those over ice and over water. The relative humidity error calculation uses recalculated RHs adding the errors from the temperature and (separately) the positive, linear value of the water vapor error (the right-hand side of Eq. 29). We report the relative humidity uncertainty as the root-sum-of-squares of the differences between these re-calculated relative humidities and the reported values.

3. Acknowledgements

We thank Sirvard Akopyan, George Aumann, Chris Barnet, Kevin Bowman, Thomas Chung, Sergio DeSouza-Machado, Dejian Fu, Antonia Gambacorta, the late John Gieselman, Mike Gunson, Chris Hepplewhite, Glynn Hulley, Ramesh Kakar, Peter Kalmus, Susan Kulawik, Bjorn Lambrigtsen, Sung-Yung Lee, Eric Maddy, Mike Newchurch, Tom Pagano, Derek Posselt, Jacola Roman, Edwin Sarkissian, Larrabee Strow, Joel Susskind, Joao Teixeira, Baijun Tian, Geoff Toon, George Wang, Tao Wang, Chris Wilson, Sun Wong, and John Worden.

In memory of Mous Chahine. Your bird still flies.

This research was performed at the Jet Propulsion Laboratory, California Institute of Technology, under contract to the National Aeronautics and Space Administration.

4. References

Aumann, H. H., Chahine, M. T., Gautier, C., Goldberg, M.D., Kalnay, E., McMillin, L. M., Revercomb, H., Rosenkranz, P.W., Smith, W. L., Staelin, D. H., Strow, L. L., and Susskind, J.: AIRS/AMSU/HSB on the Aqua mission: design, science objectives, data products, and processing systems, IEEE Trans. Geosci. Remote Sensing, 41, 253-264, 2003.

Barnet, C., Manning, E., Rosenkranz, P., Strow, L., Susskind, J., and Chahine, M.T.:"AIRS Level 2 Algorithm Theoretical Basis Document Version 4.0," (H. A. Aumann, ed.), available at https://eospso.gsfc.nasa.gov/sites/default/files/atbd/20070301_L2_ATBD_signed.pdf, 2007.

Baum, B. A., Yang, P., Nasiri, S., Heidinger, A. K., Heymsfield, A., and Li, J.: Bulk scattering properties for the remote sensing of ice clouds. Part III: High-resolution spectral models from 100 to 3250 cm^{-1}, J. Appl. Meteorol. Climatol., 46, 423–434, 2007.

Bowman, K. W., Rodgers, C. D., Kulawik, S. S., Worden, J., Sarkissian, E., Osterman, G., Steck, T., Luo, M., Eldering, A., Shephard, M., Worden, H., Lampel, M., Clough, S., Brown, P., Rinsland, C., Gunson, M., and Beer, R.: Tropospheric Emission Spectrometer: Retrieval method and error analysis, IEEE Trans. Geosci. Remote Sensing, 44, 1297-1307, 2006.

Chahine, M. T., AIRS: Improving weather forecasting and providing new data on greenhouse gases. *Bull. Amer. Met. Soc.*, 87, 911-926, 2006.

DeSouza-Matchado, S., Strow, L. L., Tangborn, A., Huang, X., Chen, X., Liu, X., Wu, W., and Yang, Q: Single footprint retrievals for AIRS using a fast TwoSlab cloud-representation model and all-sky radiative algorithm, Atmos. Meas. Tech.., doi:10.5194/amt-11-529-2018, 2018.

Irion, F. W., Kahn, B. H., Schreier, M. M., Fetzer, E. J., Fishbein, E., Fu, D., Kalmus, P., Wilson, R. C., Wong, S., and Yue, Q.: Single-footprint retrievals of temperature, water vapor and cloud properties from AIRS, Atmos. Meas. Tech., 11, 971-995, doi:10.5194/amt-11-971-2018, 2018.

Jin, H., and Nasiri, S. L., Evaluation of AIRS Cloud-Thermodynamic-Phase Determination with CALIPSO, J. Appl. Meteorol. Clim., 53, 1012-1027, doi:10.1175/JAMC-D-13-0137.1, 2013.

Kahn, B. H., and Teixeira, J.: A Global Climatology of Temperature and Water Vapor Variance Scaling from the Atmospheric Infrared Sounder, J. Climate, 22, 5558-5576, 2009.

Kahn, B. H., Irion, F. W., Dang, V. T., Manning, E. M., Nasiri, S. L., Naud, C. M., Blaisdell, J. M., Schreier, M. M., Yue, Q., Bowman, K. W., Fetzer, E. J., Hulley, G. C., Liou, K. N., Lubin D., Ou, S. C., Susskind, J. , Takano, Y., B. Tian, B., and Worden, J. R.: The Atmospheric Infrared Sounder version 6 cloud products, Atmos. Chem. Phys., 14, 399-426, doi:10.5194/acp-14-399-2014, 2014.

Kulawik, S. S., Osterman, G., Jones, D. B. A., and Bowman, K. W.: Calculation of altitude-dependent Tikhonov constraints for the TES nadir retrievals, IEEE Trans. Geosci. Remote Sensing, 44, 1334-1342, 2006.

McPeters, R. D., Labow, G. J., and Logan, J. A.: Ozone climatological profiles for satellite retrieval algorithms, J. Geophys. Res., 112, D05308, doi:10.1029/2005JD006823, 2007.

Mishchenko, M. I., Travis, L. D., and Lacis, A. A.: "Scattering, Absorption, and Emission of Light by Small Particles", Cambridge University Press, Cambridge, 2002.

Moré, J. J.: The Levenberg-Marquardt algorithm: implementation and theory, in: Numerical analysis (Proc. 7th Biennial Conf., Univ. Dundee, Dundee, 1977), Lecture Notes in Math., Vol. 630, Springer, Berlin, 105–116, 1978.

Murray, F. W.: On the Computation of Saturation Vapor Pressure, J. Appl. Meteorol. Clim, 6(1), 203-204, doi.org/10.1175/1520-0450(1967)006<0203:OTCOSV>2.0.CO;2, 1967.

Ou, S. S. C., Kahn, B. H., Liou, K.-N., Takano, Y., Schreier, M. M., and Yue, Q.: Retrieval of cirrus cloud properties from the Atmospheric Infrared Sounder: The k-coefficient approach using cloud-cleared radiances as input, IEEE Trans. Geosci. Remote Sensing, 51, 1010-1024, 2013.

Pagano, T., "Estimation of AIRS correlated noise," AIRS Design File Memo ADFM-614, AIRS Project Office, Jet Propulsion Laboratory, Pasadena CA, 2002.

Pagano, T. S., Aumann, H. H., Hagan, D. E., and Overoye, K.: Prelaunch and in-flight radiometric calibration of the Atmospheric Infrared Sounder (AIRS), IEEE Trans. Geosci. Remote Sensing, 41, 265-273, 2003.

Pagano, T. S., Aumann, H. H., Manning, E. M., Elliott, D. A., and Broberg, S. E.: Improving AIRS radiance spectra in high contrast scenes using MODIS, Proc. SPIE 9607, Earth Observing Systems XX, doi:10.1117/12.2188311, 2015.

Platnick, S., Meyer, K. G., King, M. D., Wind, G., Amarasinghe, N., Marchant, B., Arnold, G. T., Zhang, Z., Hubanks, P. A., Holz, R. E., Yang, P., Ridgway, W. L., and Riedi, J.: The MODIS Cloud Optical and Microphysical Products: Collection 6 Updates and Examples From Terra and Aqua, IEEE Trans. Geosci. Remote Sensing, 55, 502 – 525, 2017.

Rodgers, C. D.: Inverse Methods for Atmospheric Sounding: Theory and Practice, World Scientific Publishing, Singapore, 2000.

Sarkissian, E.: The Levenberg–Marquardt algorithm for solving the nonlinear least squares problem: Theory, implementation and application, M.S. thesis, California State University, Los Angeles, 2001.

Schreier, M. M., Kahn, B. H., Eldering, A., Elliott, D. A., Fishbein, E., Irion, F. W., and Pagano, T. S.: Radiance comparisons of MODIS and AIRS using spatial response information, J. Atmos. Ocean. Tech., 27, doi: 10.1175/2010JTECHA1424.1, 2010.

Seeman, S. W., Borbas, E. E., Knuteson, R. O, Stephenson, G. R., and Huang, H.-L.: Development of a Global Infrared Land Surface Emissivity Database for Application to Clear Sky Sounding Retrievals from Multispectral Satellite Radiance Measurements, J. Appl. Met. Clim., 47, 108-123, doi: 10.1175/2007JAMC1590.1, 2008.

Strow, L. L., Hannon, S. E., De Souza-Machado, S., Motteler, H. E. and Tobin, D.: An Overview of the AIRS Radiative Transfer Model, IEEE Trans. Geosci. Remote Sensing, 41, 303-313, 2003.

Strow, L. L., Hannon, S. E., De Souza-Machado, S., Motteler, H. E. and Tobin, D. C.: Validation of the Atmospheric Infrared Sounder radiative transfer algorithm, J. Geophys. Res., 111, D09S06, doi: 10.1029/2005JD006146, 2006.

Tobin, D. C., Antonelli, P., Revercomb, H. E., Dutcher, S., Turner, D. D., Taylor, J. K., Knuteson, R. O., and Vinson, K., Hyperspectral data noise characterization using principle component analysis: application to the Atmospheric Infrared Sounder, J. Appl. Remote Sens., 1, 013515, doi: 10.1117/1.2757707, 2007.

van Delst, P.: JCSDA infrared sea surface emissivity model, in Proceedings of the 13th International TOVS study conference, Sainte-Adèle, Québec, Canada, 2003.

Wagner, W., and Pruß, A.: The IAPWS Formulation 1995 for the Thermodynamic Properties of Ordinary Water Substance for General and Scientific Use, J. Phys. Chem. Ref. Data, 31, 387-535, 2002.

Wang, L., Trembley, D., Zhang, B., and Han, Y., Fast and Accurate Collocation of the Visible Infrared Imaging Radiometer Suite Measurements with Cross-Track Infrared Sounder, *Remote Sens.*, *8*, 76; doi:10.3390/rs8010076, 2016.

Weiler, M. H., Overoye, K. R., Stobie, J. A., O'Sullivan, P. B., Gaiser, S. L., Broberg, S. E., and Elliot, D. A.: Performance of the Atmospheric Infrared Sounder (AIRS) in the radiation environment of low-Earth orbit, in "Earth Observing Systems X" (J. J. Butler, ed.), Proceedings of SPIE 5882, 588210, doi:10.1117/12.615244, 2005.

Wunch, D., Toon, G. C., Blavier, J.-F. L., Washenfelder, R. A., Notholt, J., Connor, B. J., Griffith, D. W. T., Sherlock, V., and Wennberg, P. O.: The Total Carbon Column Observing Network, Phil. Trans. R. Soc. A, 369, 2087–2112, 2011.